Supplementary Materials

Characterization of the cys mutants: Purification of the cysteine mutants in the apo form involves isolation of the protein from inclusion bodies followed by *in vitro* refolding (Jennings et al. 1995). Since the amino acid sequence defines the final three-dimensional structure of a protein (Anfinsen et al. 1973), mutation of native residues can alter the folding mechanism favoring alternative pathways, which may result in the formation of misfolded and aggregated species. Thus, it is essential to detect and remove such aggregates after *in vitro* refolding. Indeed elution profiles from size exclusion chromatography for some of the myoglobin mutants prepared clearly revealed the presence of a second high molecular weight but soluble species eluting at the void volume (Figure S1B). Denaturing SDS-PAGE electrophoresis revealed that the molecular mass of the species eluting at the void volume corresponds to that of myoglobin (Figure S1C). It is emphasized that refolding was done in the presence of DTT, hence eliminating disulfide formation between monomers as the source of misfolding and subsequent oligomerization. Interestingly, mutants R118C, A127C, and K133C resulted in 100% oligomer formation (Figure S1D) and were not further investigated.

The misfolded oligomeric species observed for some of the mutants in this work are likely different from the soluble aggregates observed in earlier studies, which revealed that *in vitro* refolding of WT apo myoglobin from inclusion bodies results in the formation of a significant fraction of aggregates with an average M_W > 1MDa that were undetected in gel filtration purification due to adsorption on the column matrix (Chow et al. 2006). It is noted that the *soluble* aggregates contribute significantly to the EPR spectra of the spin-labeled samples (Figure S2), which shows the importance of removing aggregated species prior to EPR data collection.

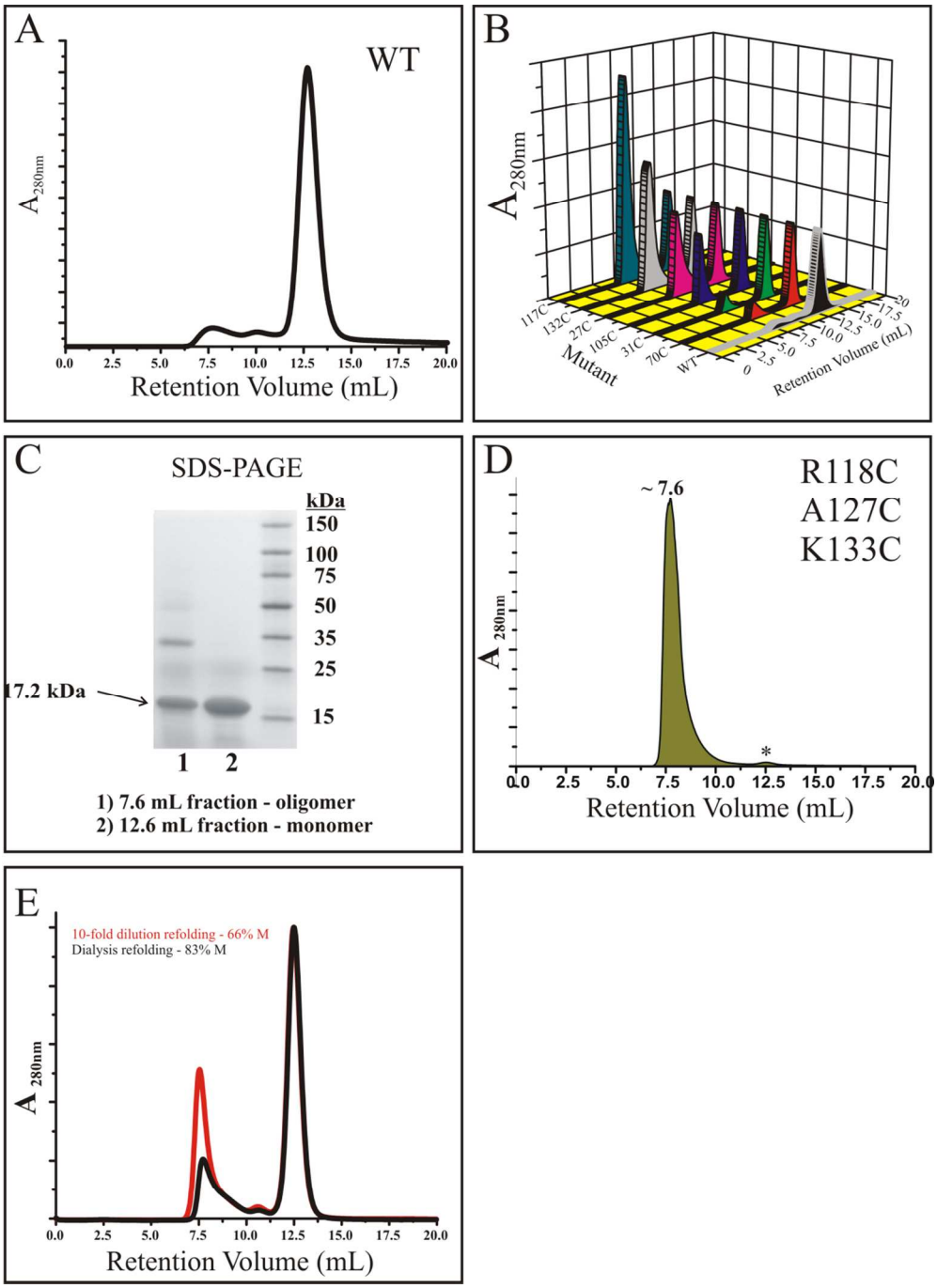

Figure S1: Elution profile from size exclusion chromatography of WT and cys myoglobin mutants. (A) WT apomyoglobin. (B) 3D-graph showing the elution profiles of WT and selected set of mutants injected in the Superdex 75 column. (C) SDS-PAGE of fractions eluted from the size exclusion column. D) Elution profiles of mutants that completely misfolded. (D) Cys mutant refolded *via* 10-fold dilution (red) or *via* overnight dialysis (black).

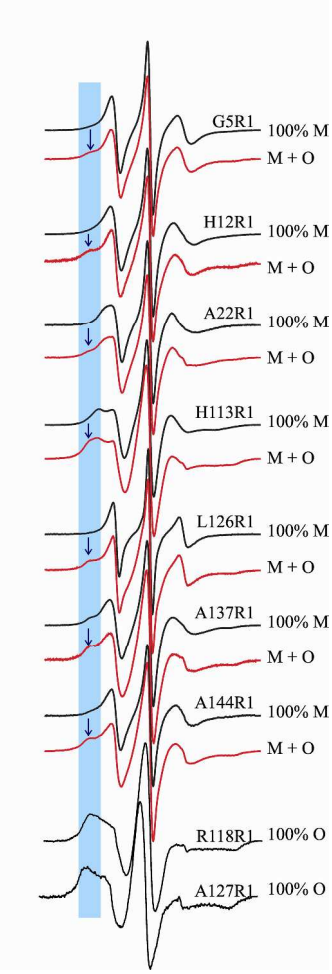

Figure S2: Contribution of oligomeric species to the EPR spectra of spin-labeled myoglobin mutants. EPR spectra of R1 mutants before and after gel filtration are shown in red and black, respectively. The arrows indicates spectral component arising due to the presence of misfolded proteins. M: monomer, O: oligomer.

CD spectroscopy: Far-UV CD measurements of WT and spin-labeled myoglobin samples were conducted at room temperature in a Jasco-810 spectropolarimeter equipped with a Peltier temperature-controlled sample holder using a cuvette with a 1 mm path length. Spectra were recorded from 190-260 nm and were an average of 4 scans. Samples consisted of 0.2 mg/ml protein in either 10mM sodium acetate, pH 6.1 buffer for N_{Apo} measurements or 10mM sodium acetate, pH 4.1 buffer for I_{MG} measurements. Chemical denaturation of myoglobin in the I_{MG} state was carried out at room temperature and the CD signal was monitored at 223 nm as a

function of guanidinium hydrochloride concentration in 10mM sodium acetate, pH 4.1 buffer with and without 25% w/w Ficoll 70 (Figure S3). The protein concentration for the chemical denaturation studies was 0.5 mg/ml. The chemical denaturation data was fit using a nonlinear extrapolation method described by Santoro and Bolen, 1988 and the results are tabulated in table S1.

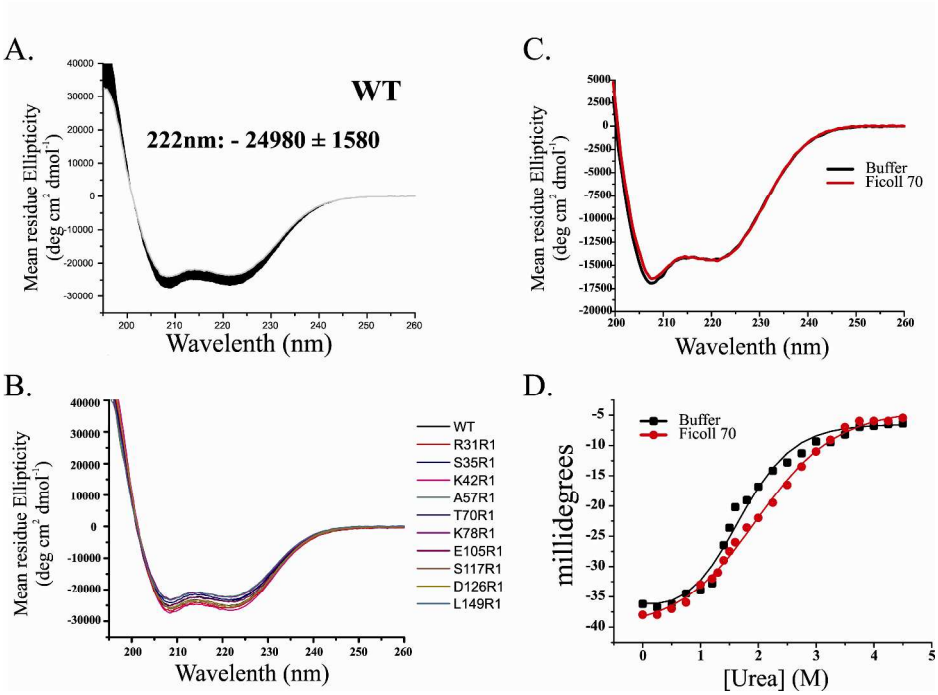

Figure S3: Effect of R1 and Ficoll 70 on the structure and stability of apomyoglobin. (A) Far-UV CD spectrum of WT myoglobin showing the standard deviation of the data based on triplicate measurements. (B) Far-UV CD spectra of R1 mutants of myoglobin in the N_{Apo} state. (C) Ficoll 70 effects on the secondary structure of myoglobin in the I_{MG} state. (D) Ficoll 70 effects on the stability of myoglobin in the I_{MG} state.

Table S1: Effect of Ficoll 70 on the stability of ApoMyb WT in the $\mathbf{I_{MG}}$ state (10mM sodium acetate pH 4)

Sample	pH	ΔG (H_2O) (kcal/mol)	*m* (kcal/mol*M)	$[Urea]_{1/2}$
Buffer	4	-1.87±0.03	1.22±0.07	1.54±0.03
Ficoll 70	4	-1.72±0.01	0.89±0.03	1.94±0.02

Change in stability of ApoMyb in Ficoll 70 solution: $\Delta\Delta G = -1.87 - (-1.72) = 0.15$ kcal/mol

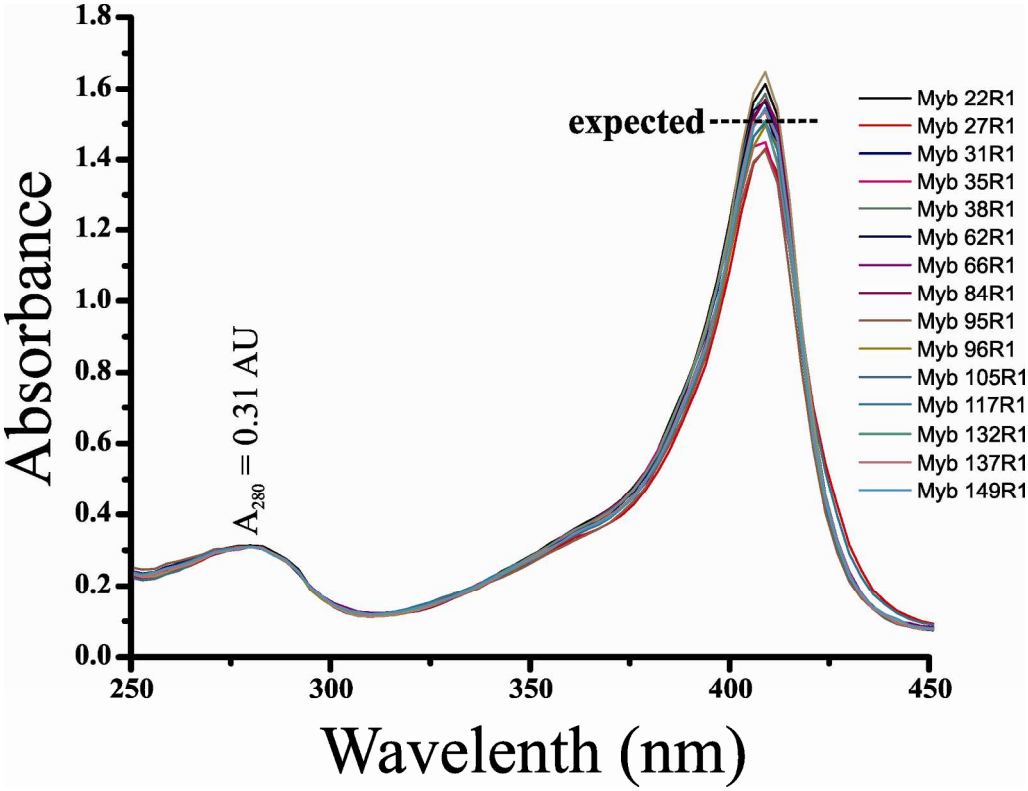

Figure S4: UV-Vis scan of a set of R1 mutants of myoglobin reconstituted with bovine heme. The spectra were normalized to the same protein concentration (10 μM) as judged by the absorption at 280 nm. The values of ε_{409} and ε_{280} are 157,000 and 31,000 M^{-1} cm^{-1}, respectively (Fasman, 1992). Thus, for the normalized A_{280} = 0.31, the expected A_{409} is 1.55.

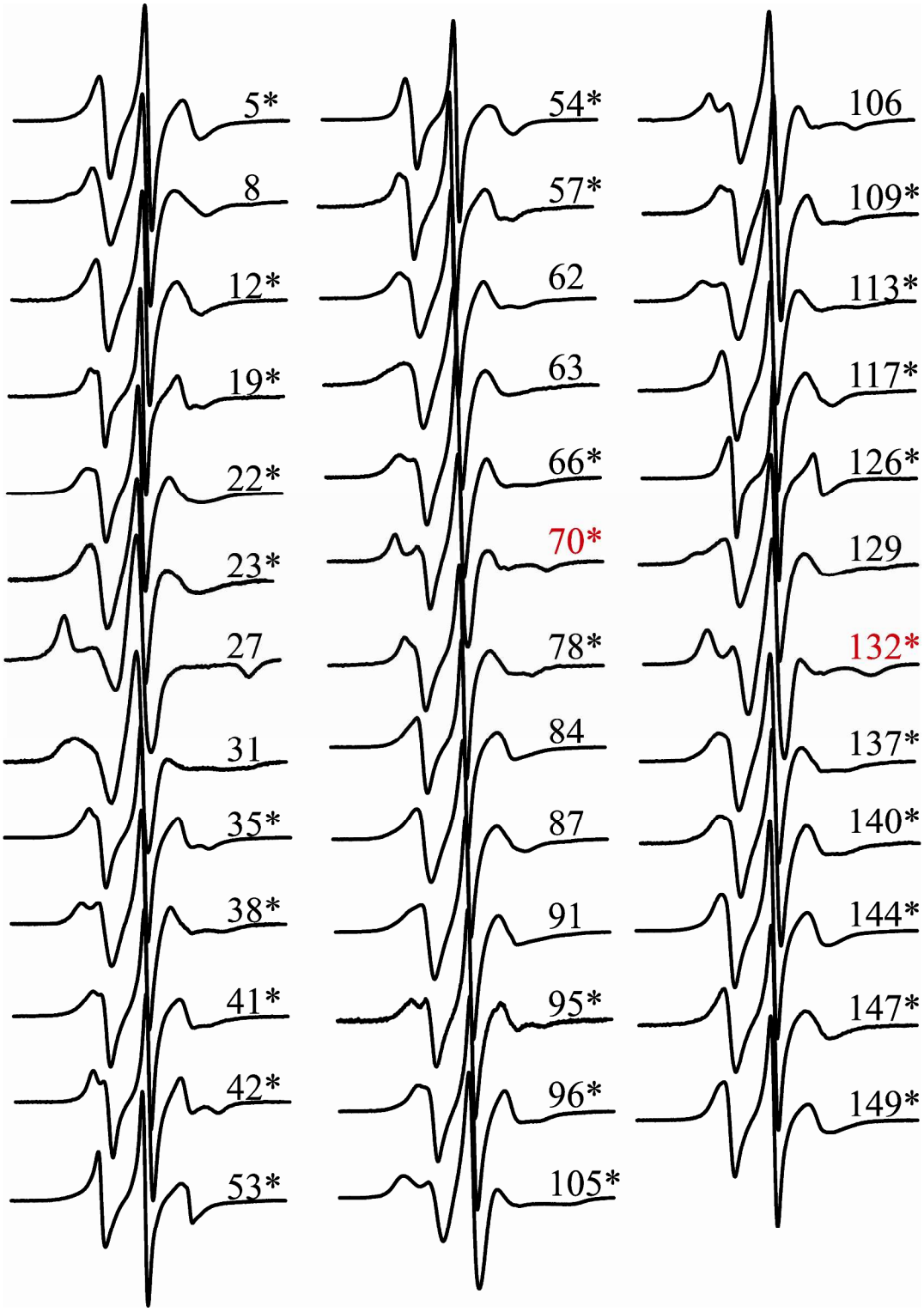

Figure S5: EPR spectra of R1 of myoglobin in the N_{Holo} state. Asterisk indicates spectra reflecting simple anisotropic motion of R1. The spectra of residues 70R1 and 132R1 (red label) reflect a single component, but of high order ($S > 0.5$; see Table S2 and Figure S6), which may arise from tertiary interaction of the nitroxide ring with the environment.

Simulation of EPR spectra of spin-labeled myoglobin mutants: EPR spectra were fit with the MOMD model of Freed and coworkers (Budil et al., 1996) using the program NLSL as previously described. The software is available at ftp://ftp.ccmr.cornell.edu/pub.freed. For all simulations, the starting values for the A and g magnetic tensor were taken as g_{xx} = 2.0078, g_{yy} = 2.0060, g_{zz} = 2.0022, and A_{xx} = 6.2, A_{yy} = 5.9, A_{zz} = 37, which correspond to a nitroxide side chain in an aqueous environment (Kusnetzow et al., 2006). Reasonable fits were obtained with an axially symmetric motion, where $R_z \equiv R_\parallel$ and $R_x = R_y \equiv R_\perp$. In a modified spherical representation, the motion is specified by the geometric mean of the diffusion rate ($\bar{R}$) and the asymmetry parameter (N), where $\bar{R} = \sqrt[3]{R_\parallel R_\perp^2}$ and $N = \frac{R_\parallel}{R_\perp}$. For z-axis anisotropic motion, the tilt angles of the diffusion tensor were set to α_D = 0 °, β_D = 36 °, γ_D = 0 ° and subject to an ordering potential described by the coefficient C_{20} from which the order parameter S is computed (Budil et al., 1996). Save for one case (see below), the relatively immobile components in the spectra were taken to have isotropic motion where N = 0. Least-square fits were obtained by variation of only $\bar{R}$, N, and C_{20} only for the mobile components and only $\bar{R}$ for the immobile states. After the above parameters were optimized, inhomogeneous linewidth (**W**) values were allowed to vary slightly to improve the fits. For R1 at non-interacting surface sites, typical values for inhomogeneous linewidth (**W**) were in the range of 0 - 0.5, while the same for relatively immobile components were in the range of 0 - 1.3. Finally, the principal values of the A and g magnetic tensor were allowed to vary slightly in order to get the final best fits. From the final fits, the effective correlation time (τ) was calculated as $\tau = \frac{1}{6\bar{R}}$ and the order parameter was computed directly from C_{20} (Budil et al., 1996). The MOMD fit for residue 66R1 in the I_{MG} state required three components, namely a highly mobile state with S = 0 in addition to two more

relatively immobilized states, each of which have an anisotropic motion of the type characteristic of helix surface sites, but with different values of S and τ.

Table S2: Dynamic parameters obtained from MOMD simulation for the indicated sites.

Folding state - Mutant		τ (ns)	S	%
N_{Holo} – 5R1		1.4	0.27	100
N_{Holo} – 12R1		1.7	0.30	100
N_{Holo} – 41R1		1.6	0.38	100
N_{Holo} – 42R1		1.8	0.46	100
N_{Holo} – 54R1		1.2	0.19	100
N_{Holo} – 57R1		1.3	0.34	100
N_{Holo} – 62R1	*m* component	1.8	0.39	88
	i component	4.8	0	12
N_{Holo} – 66R1		2.2	0.45	100
N_{Holo} – 70R1		2.4	0.60	100
N_{Holo} – 78R1		1.5	0.43	100
N_{Holo} – 87R1	*m* component	2.3	0.24	90
	i component	7.2	0	10
N_{Holo} – 106R1	*m* component	1.8	0.61	93
	i component	12.9	0	7
N_{Holo} – 109R1		2.0	0.37	100
N_{Holo} – 113R1		2.3	0.50	100
N_{Holo} – 132R1		3.7	0.68	100
N_{Holo} – 137R1		2.2	0.37	100
N_{Holo} – 144R1		1.7	0.28	100
N_{Holo} – 147R1		1.5	0.29	100
N_{Apo} – 42R1	*m* component	2.2	0.31	45
	i component	6.2	0	55
N_{Apo} – 78R1	*m* component	1.8	0.27	62
	i component	6.9	0	38
N_{Apo} – 106R1	*m* component	1.7	0.36	56
	i component	5.6	0	44
I_{MG} – 66R1	*m* component	0.7	0	17
	i-1 component	1.9	0.28	21
	i-2 component	3.2	0.49	62
I_{MG} – 113R1	*m* component	2.3	0.26	42
	i component	5.9	0	58

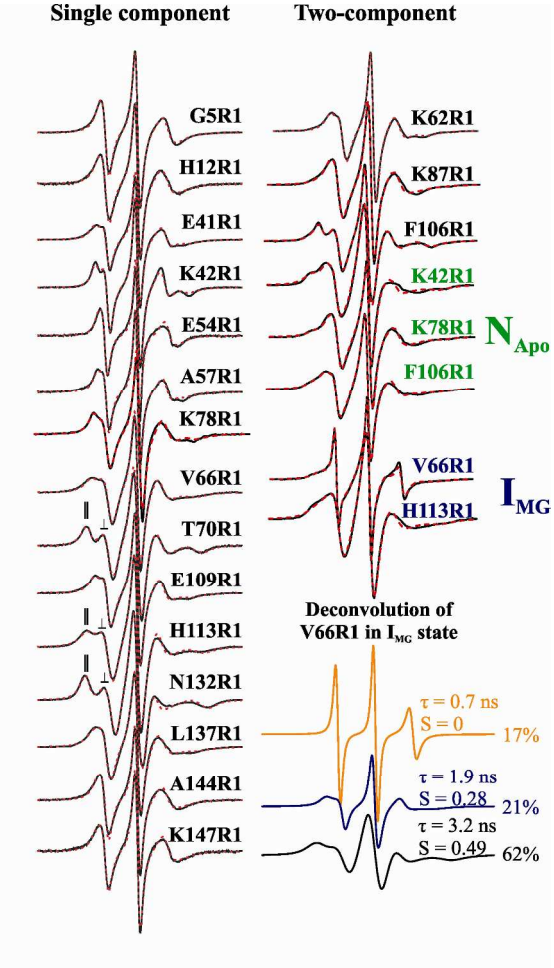

Figure S6: MOMD fits of a set EPR spectra of R1 at the indicated states. The experimental (black trace) and simulated (dashed red trace) spectra are overlaid. The black, green, and dark blue labels identify spectra recorded in the N_{Holo}, N_{Apo}, and I_{MG} states, respectively. The parameters for the three components obtained from MOMD fit of 66R1 in I_{MG} state are shown.

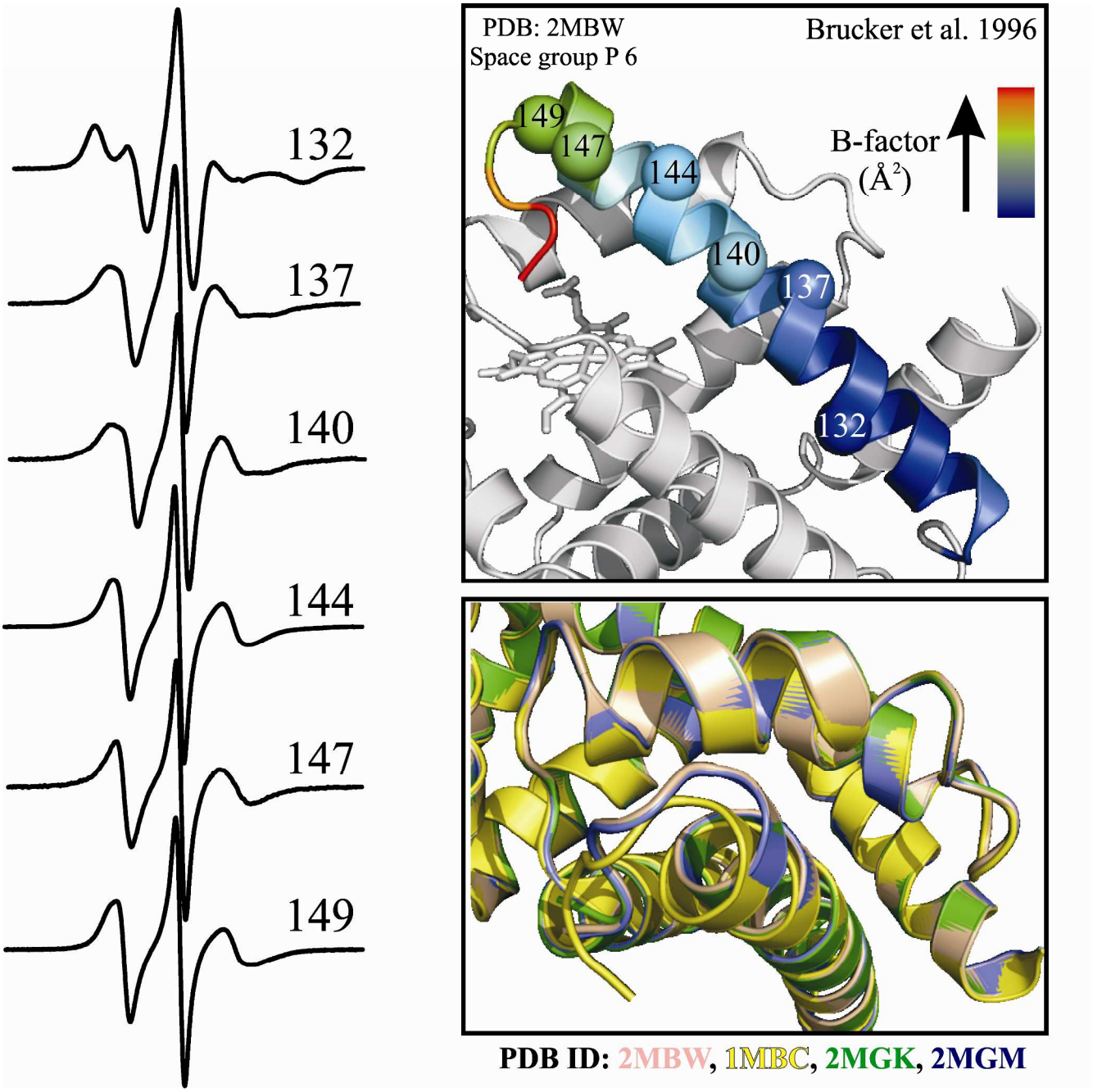

Figure S7: Mobility gradient of R1 within the H-helix likely reflects local segmental ns time scale motions within the helix. *Left panel*: EPR spectra of R1 at sites within the H-helix. *Top right panel*: Ribbon diagram of myoglobin (PDB code 2MBW) color coded based on B-factors values (Brucker et al. 1996). *Bottom right panel*: Overlay of high-resolution structures of myoglobin showing plasticity of the c-terminal region of the helix (Brucker et al. 1996; Kuriyan et al. 1986; Quillin et al. 1993).

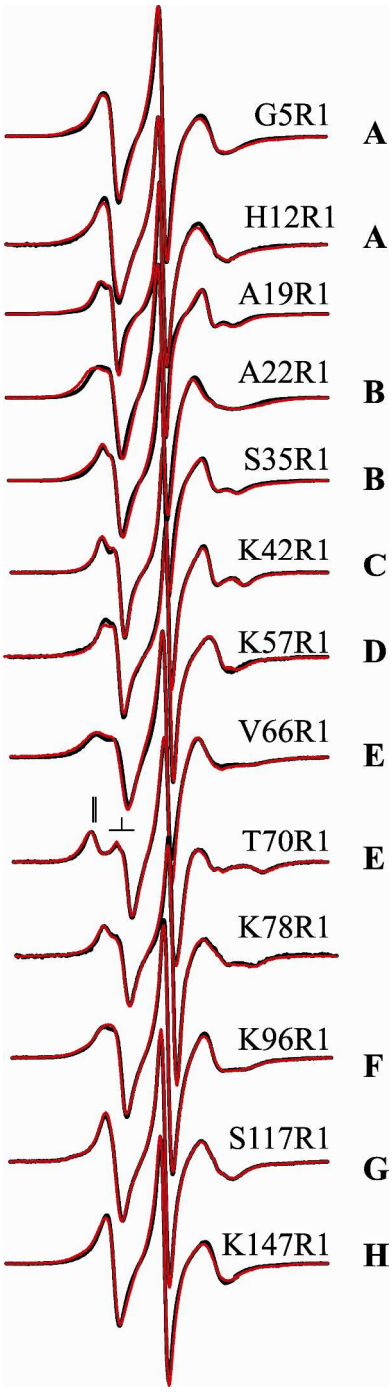

Figure S8: Sites that show a single component spectrum in the N_{Holo} state do not show an osmolyte shift. The EPR spectra recorded in Ficoll (black) and sucrose (red) are overlaid. The helix in which each R1 side chain is located at is indicated. The subtle lineshape change at site A22R1 in sucrose correspond to a small change in the ns mobility of the nitroxide that may reflect viscous damping of ns local backbone modes.

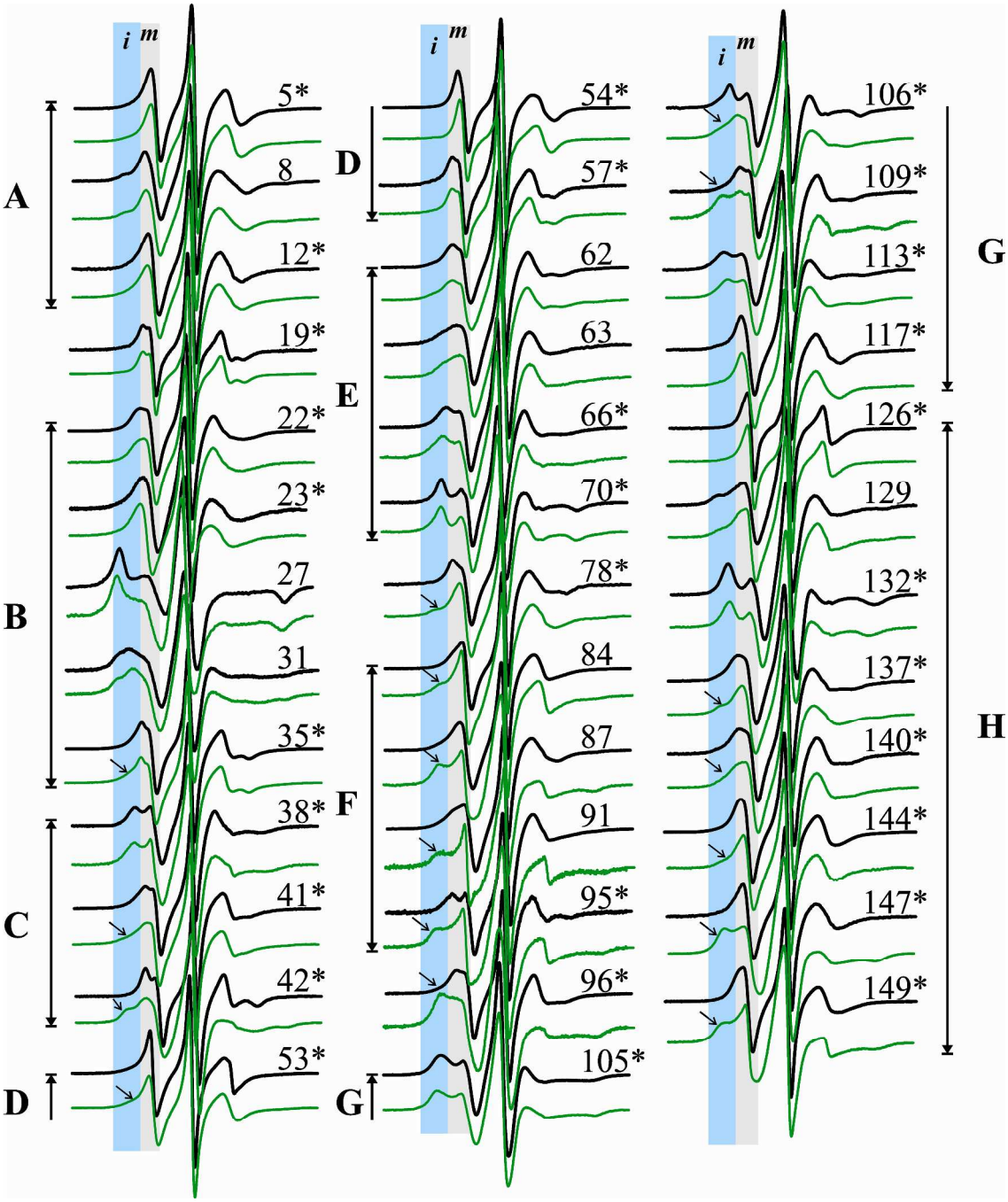

Figure S9: EPR spectra of R1 at the indicated sites in the N_{Holo} (black) and N_{Apo} (green) state. The asterisks identify the sites reflecting a single dynamic state in the N_{Holo} state. Arrows are used to identify a new relatively immobilized component observed in the N_{Apo} state. The helix in which each R1 mutant is located at is indicated. The EPR spectra of residues 41R1, 66R1, 84R1, 87R1, 91R1 and 96R1 N_{Apo} state have been reported (López et al. 2009; Armstrong et al. 2011) and are reproduced here.

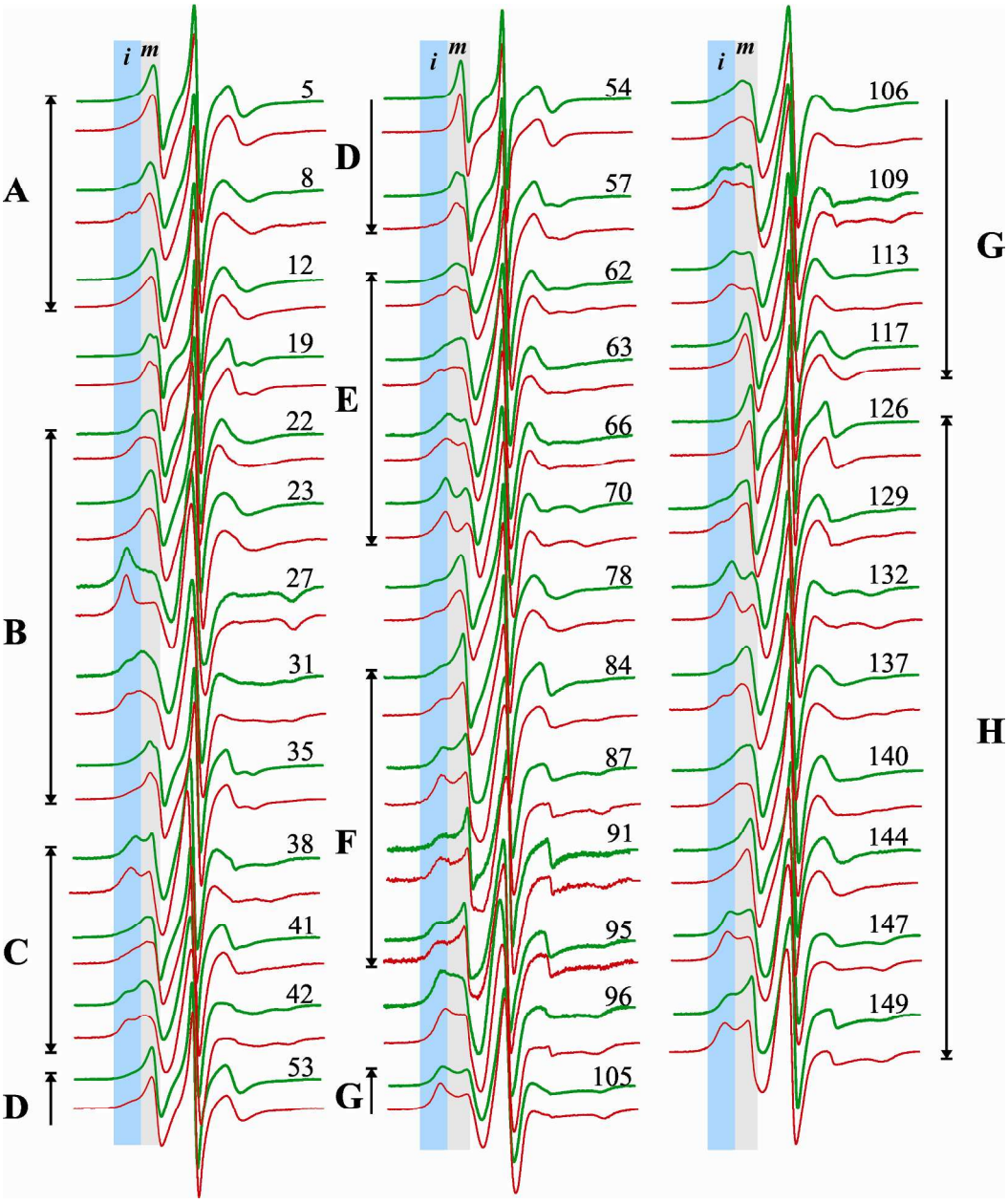

Figure S10: Mapping the conformational flexibility of myoglobin in the N_{Apo} state with osmolyte perturbation SDSL. EPR spectra of R1 mutants of myoglobin in the N_{Apo} state recorded in Ficoll 70 (green) and in sucrose (red). The light blue and gray areas identify spectral intensities corresponding to relatively immobile and mobile states of the nitroxide, respectively. The helix in which each R1 mutant is located at is indicated.

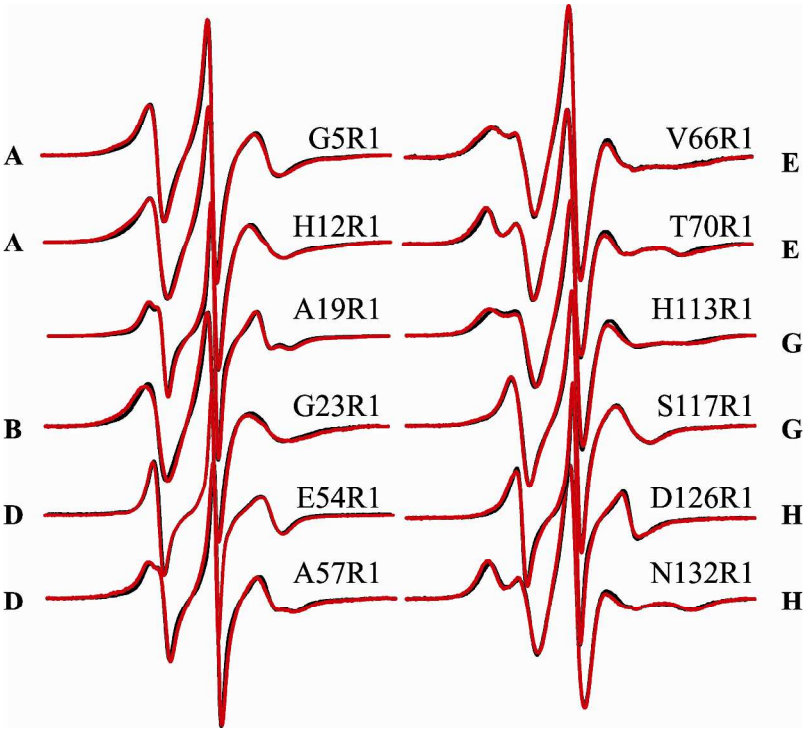

Figure S11: Sites that show a single component spectrum in the N_{Apo} state do not show an osmolyte shift. The EPR spectra recorded in Ficoll (black) and sucrose (red) are overlaid. The helix in which each R1 side chain is located at is indicated. The subtle lineshape change at sites G23R1 and H113R1 in sucrose correspond to a small change in the ns mobility of the nitroxide that may reflect viscous damping of ns local backbone modes.

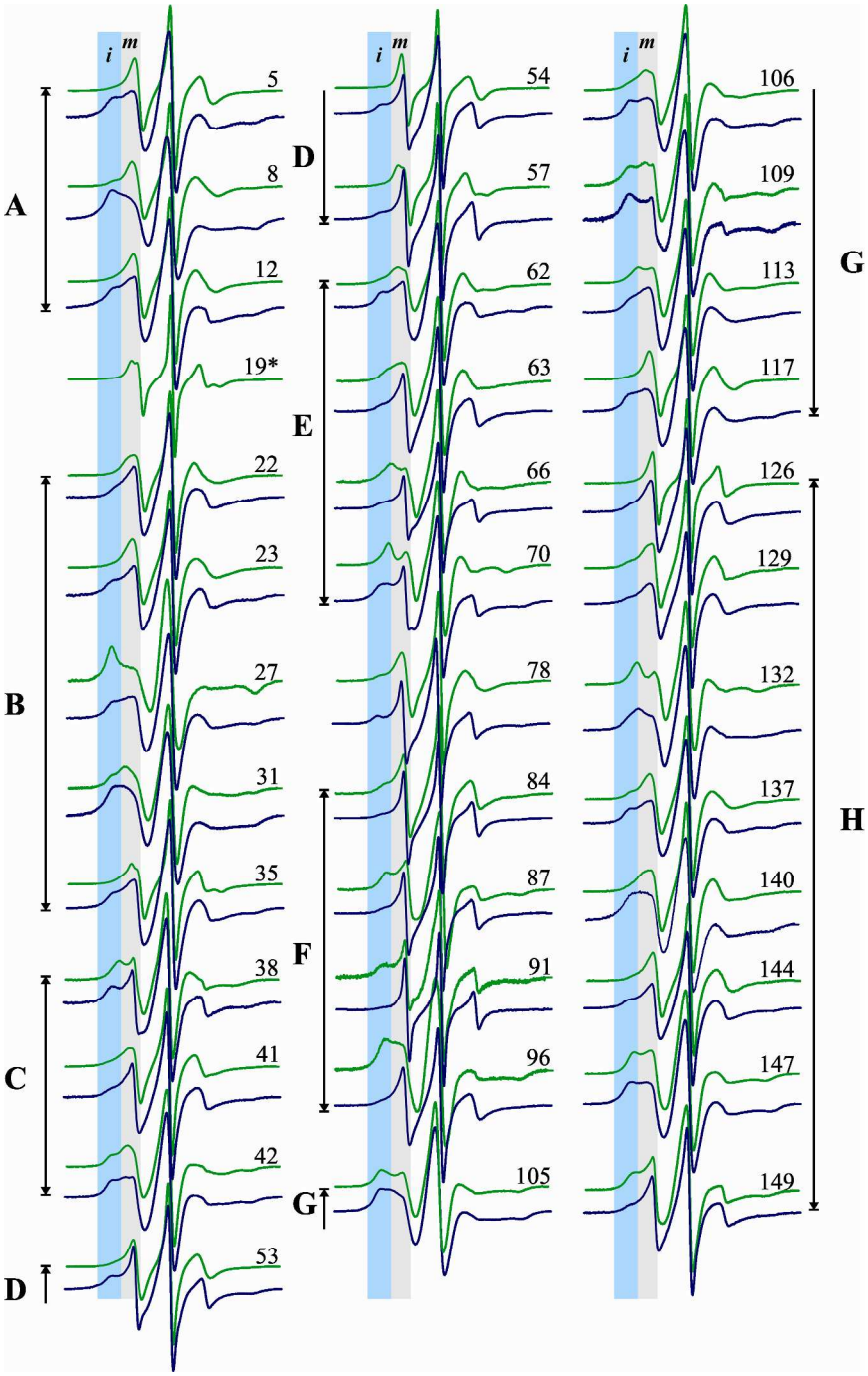

Figure S12: EPR spectra of R1 at the indicated sites in the N_{Apo} (green) and I_{MG} (blue) state. The EPR spectrum of residue A19R1 in the I_{MG} state (*) is not shown due to the presence of aggregates in the sample. The EPR spectrum of the monomeric species is shown in Figure S13 below. The helix in which each R1 mutant is located at is indicated. The EPR spectra of residues 41R1 and 66R1 in Ficoll have been reported (Armstrong et al. 2011) and are reproduced here

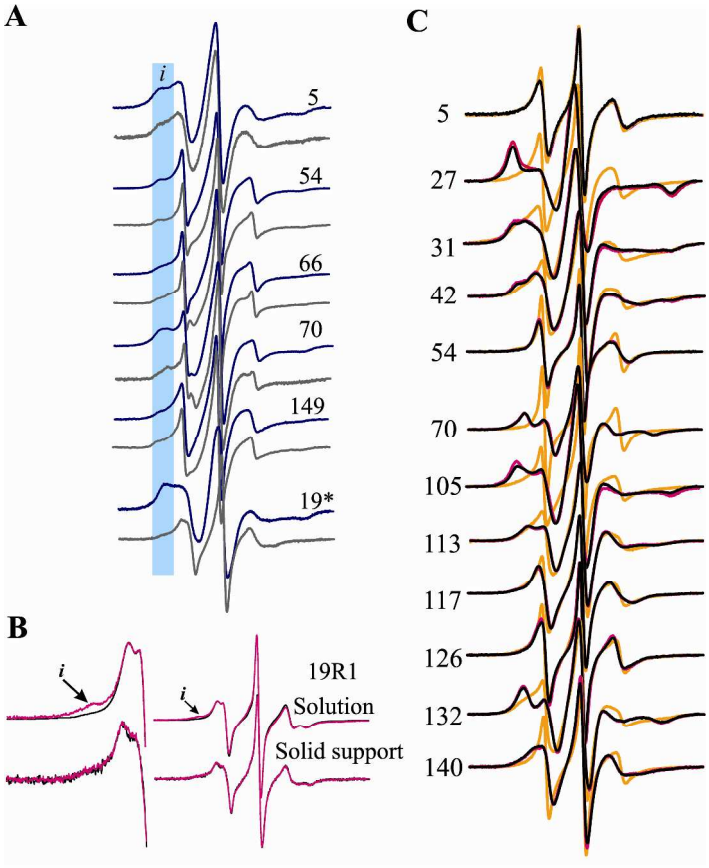

Figure S13: Use of solid support EPR to test whether the *i* component observed in the EPR spectra of R1 in the I_{MG} state arise due to soluble aggregates. A) EPR spectra of a set myoglobin mutants immobilized on a Sepharose solid support (see *Methods*) prior to populating the I_{MG} state are shown in dark gray. The EPR spectra of the same samples in Ficoll 70 solutions are shown for comparison (blue). The shaded area identify region of spectral intensity corresponding to the relatively immobilized component. B) EPR spectra of residue 19R1 in the N_{Apo} state in solution and in the solid support prior to acid unfolding (black) and after refolding (magenta). The low field peaks for both spectra are enlarged for clarity. The new *i* component likely arising due to aggregation in the solution sample is highlighted (see arrow). C) pH reversibility of spin-labeled myoglobin mutants. EPR spectra of the indicated mutant in the N_{Apo} state prior to acid unfolding (black), the acid unfolded state (pH 2.3; orange), and refolded (N_{Apo}) from the acid unfolded state (magenta) are superimposed. Due to the incompatibility of Ficoll 70 with acid pH, the spectra in the acid unfolded state (pH 2.3) were recorded in sucrose.

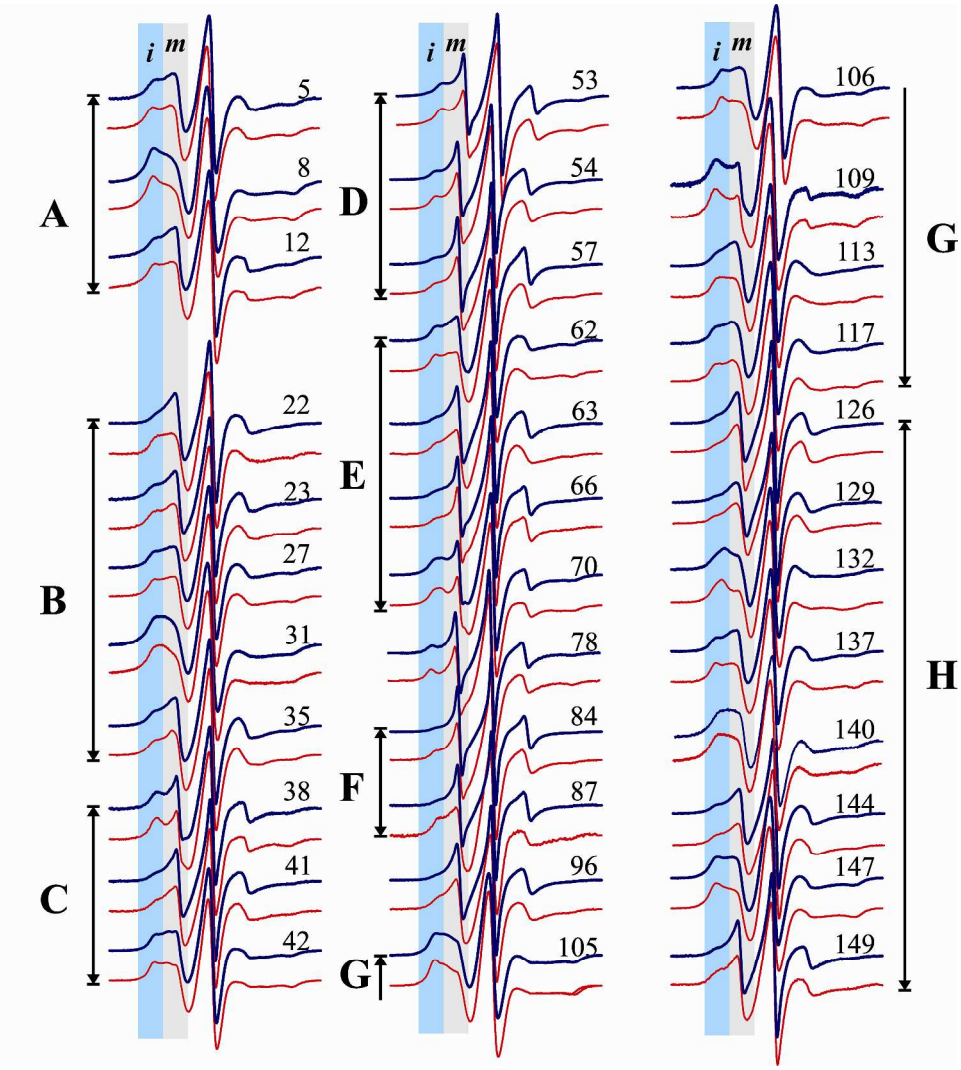

Figure S14: Mapping the conformational flexibility of myoglobin in the I_{MG} state with osmolyte perturbation SDSL. EPR spectra of R1 mutants of myoglobin in the I_{MG} state recorded in Ficoll 70 (blue) and in sucrose (red). The light blue and gray areas identify spectral intensities corresponding to relatively immobile and mobile states of the nitroxide, respectively.

Modeling of the R1 side chain on the structure of myoglobin: The R1 side chain was modeled at sites 31R1, 57R1, 70R1, 87R1, and 132R1 in the high-resolution x-ray structure (PDB ID: 2MBW) using DS Viewer Pro 5.0 software (Accelrys, Inc). The $X_1 - X_3$ dihedral angles modeled were those previously observed at helical sites in crystals structures of T4 lysozyme (Langen et al., 2000; Guo et al., 2007; Guo et al., 2008; Fleissner et al., 2009); either {-60, -60, X_3}, {180, -60, X_3}, or {180, 60, X_3}, where X_3 is ± 90°. In each case, the X_4 and X_5 rotamers modeled were those reported by Guo et al., 2008. For each site, a particular R1 rotamer was selected such that there are no steric clashes or overlap on the nitroxide side chain with the rest of the molecule.

Table S3: Most probable interspin distance and distance distributions for R1 doubles of myoglobin in the N_{Holo}, N_{Apo}, and I_{MG} states.

Mutant	Helices	R1-R1 distance from modeling[†] (Å)	Most probable R1-R1 distance from DEER (Å)	Width of distance distribution from DEER[‡] (Å)
12R1/132R1 N_{Holo}	A/H	25	23.7	5.8
12R1/132R1 N_{Apo}		-	24.3	5.8
12R1/132R1 I_{MG}		-	24.3	~14.0
31R1/70R1 N_{Holo}	B/E	28	27.3	4.3
31R1/70R1 N_{Apo}		-	27.6	9.2
31R1/87R1 N_{Holo}	B/F	39	36.7	11.0
31R1/87R1 N_{Apo}		-	20.2 $^{53\%}$ & 36.0 $^{47\%}$	10.0 & 14.5
57R1/132R1 N_{Holo}	D/H	33	34.1	3.9
57R1/132R1 N_{Apo}		-	34.1	4.4

[†] Estimates of inter-nitroxide distances from modeling the R1 side chain in the crystal structure of the holo protein (PDB ID: 2MBW)

[‡] Width of the distribution taken as R1-R1 distances between 16 to 84% probability

Supplementary references:

1. Jennings, P.A. Stone, M.J., Wright, P.E. (1995) Overexpression of myoglobin and assignments of it amide, C^{α} and C^{β} resonances. *J. Biomol. NMR*. 6: 271-276.
2. Anfinsen, C.B. (1973) Principles that govern the folding of protein chains. *Science* 181:223-230.
3. Chow, C., Kurt, N., Murphy, R.M., and Cavagnero, S. (2006) Structural characterization of apomyoglobin self-associated species in aqueous buffer and urea solution. *Biophys. J.* 90:298-309.
4. Santoro M.M, and Bolen, D.W. (1988) Unfolding free energy changes determined by the linear extrapolation method. 1. Unfolding of phenylmethanesulfonyl α-chymotrypsin using different denaturants. *Biochemistry* 27:8063-8068
5. Fasman G.D. (1992) *Practical handbook of biochemistry and molecular biology*. CRC Press. Boca Raton, Fl.
6. Budil, D.E., Lee, S., Saxena, S., and Freed, J.H. (1996) Nonlinear-least-squares analysis of slow-motion EPR spectra in one and two dimensions using a modified Levenberg-Marquard algorithm. *J. Magn. Reson. Series A* 120:155-189.
7. Kusnetzow, A., Altenbach, C., and Hubbell W.L. (2006) Conformational states and dynamics of rhodopsin in micelles and bilayers. *Biochemistry* 45: 5538-5550.
8. Brucker, E.A., Olson, J.S., Phillips Jr., G.N., Dou, Y., and Ikeda-Saito, M. (1996) High resolution crystal structures of the deoxy, oxy, and aquomet forms of cobalt myoglobin. J.Biol.Chem. 271: 25419-25422
9. Kuriyan, J., Wilz, S., Karplus, M., and Petsko, G.A. (1986) X-ray structure and refinement of carbon-monoxy (Fe II)-myoglobin at 1.5 A resolution. *J.Mol.Biol*. 192:133-154

10. Quillin, M.L., Arduini, R.M., Olson, J.S., and Phillips Jr., G.N., (1993) High-resolution crystal structures of distal histidine mutants of sperm whale myoglobin. *J.Mol.Biol*. 234:140-155.

11. López, C.J., Fleissner, M.R., Guo, Z., Kusnetzow, A.K., Hubbell, W.L. (2009) Osmolyte perturbation reveals conformational equilibria in spin-labeled proteins. *Protein Sci* 18:1637-1652.

12. Armstrong, B.D., Choi, J., López, C., Wesener, D.A., Hubbell, W., Cavagnero, S., and Han, S. (2011) Site-specific hydration dynamics in the nonpolar core of a molten globule by dynamic nuclear polarization of water. *JACS* 113:5987-5995.

13. Langen, R., Oh, K.J., Cascio, D., and Hubbell, W.L. (2000) Crystal structures of spin labeled T4 lysozyme mutants: Implications for the interpretation of EPR spectra in terms of structure. *Biochemistry* 39:8396-8405.

14. Guo, Z., Cascio, D., Hideg, K., Kálai, T., and Hubbell W.L. (2007) Structural determinants of nitroxide motion in spin-labeled proteins: Tertiary contact and solvent-inaccessible sites in helix G of T4 lysozyme. *Protein Science* 16:1069-1086.

15. Guo, Z., Casio, D., Hideg, K., and Hubbell, W.L. (2008) Structural determinants of nitroxide motion in spin-labeled proteins: Solvent-exposed sites in helix B of T4 lysozyme. *Protein Science* 17:228-239.

16. Fleissner, M.R., Cascio, D., and Hubbell, W.L. (2009) Structural origins of weakly ordered motion in spin-labeled proteins. *Protein Science*. 18:893-908.